AGU PUBLICATIONS

Journal of Advances in Modeling Earth Systems

RESEARCH ARTICLE

10.1002/2017MS001003

Key Points:
- Demonstration of dynamical downscaling of a robustly chosen data set with prior bias correction of LBCs
- Inconsistencies between the impact of bias correction of LBCs prior to and after downscaling
- Bias correction of a subset of LBC variables does not guarantee improved downscaling

Correspondence to:
A. Sharma,
a.sharma@unsw.edu.au

Citation:
Benson Moalafhi, D., A. Sharma, J. Peter Evans, R. Mehrotra, and E. Rocheta (2017), Impact of bias-corrected reanalysis-derived lateral boundary conditions on WRF simulations, *J. Adv. Model. Earth Syst.*, *9*, 1828–1846, doi:10.1002/2017MS001003.

Received 4 APR 2017
Accepted 10 JUL 2017
Accepted article online 13 JUL 2017
Published online 3 AUG 2017

Impact of bias-corrected reanalysis-derived lateral boundary conditions on WRF simulations

Ditiro Benson Moalafhi[1,2], Ashish Sharma[2], Jason Peter Evans[3], Rajeshwar Mehrotra[2], and Eytan Rocheta[2]

[1]Department of Environmental Science, University of Botswana, Gaborone, Botswana, [2]School of Civil and Environmental Engineering, University of New South Wales, Sydney, New South Wales, Australia, [3]Climate Change Research Centre, University of New South Wales, Sydney, New South Wales, Australia

Abstract Lateral and lower boundary conditions derived from a suitable global reanalysis data set form the basis for deriving a dynamically consistent finer resolution downscaled product for climate and hydrological assessment studies. A problem with this, however, is that systematic biases have been noted to be present in the global reanalysis data sets that form these boundaries, biases which can be carried into the downscaled simulations thereby reducing their accuracy or efficacy. In this work, three Weather Research and Forecasting (WRF) model downscaling experiments are undertaken to investigate the impact of bias correcting European Centre for Medium range Weather Forecasting Reanalysis ERA-Interim (ERA-I) atmospheric temperature and relative humidity using Atmospheric Infrared Sounder (AIRS) satellite data. The downscaling is performed over a domain centered over southern Africa between the years 2003 and 2012. The sample mean and the mean as well as standard deviation at each grid cell for each variable are used for bias correction. The resultant WRF simulations of near-surface temperature and precipitation are evaluated seasonally and annually against global gridded observational data sets and compared with ERA-I reanalysis driving field. The study reveals inconsistencies between the impact of the bias correction prior to downscaling and the resultant model simulations after downscaling. Mean and standard deviation bias-corrected WRF simulations are, however, found to be marginally better than mean only bias-corrected WRF simulations and raw ERA-I reanalysis-driven WRF simulations. Performances, however, differ when assessing different attributes in the downscaled field. This raises questions about the efficacy of the correction procedures adopted.

1. Introduction

Dynamical downscaling offers an opportunity to study climate processes at finer detail than is currently resolved by general circulation models (GCMs) or global reanalyses [*Li et al.*, 2015; *Pohl et al.*, 2014]. These finer details are directly relevant to end users for many decision-making, planning, and development of adaptation strategies. In dynamical downscaling, output from the coarse GCM/global reanalysis is used to provide initial and lateral boundary conditions (LBCs) to a regional climate model (RCM). The ability of RCMs to convert coarser global reanalysis products to finer resolutions contributes to more realistic simulations of climate systems and processes that are relevant to hydrological applications [*Druyan and Fulakeza*, 2013; *Teutschbein and Seibert*, 2012; *Bastola and Misra*, 2013]. RCMs have become widely used tools to provide high-resolution information on the properties of a range of climate variables. The resultant finer resolution data sets could offer proxy observations for data poor regions. Among the commonly used RCMs is the Weather Research and Forecasting model (WRF) [*Skamarock et al.*, 2008]. WRF is a state of the art next-generation mesoscale model that has done well in handling regional-scale processes at finer resolutions. Its application as a RCM over southern Africa is also quite noticeable [*Pohl et al.*, 2014; *Vigaud et al.*, 2012; *Boulard et al.*, 2012], with demonstrations of its capabilities for a wide range of beneficial applications.

Although the ability of RCMs to reproduce observed characteristics has improved significantly over the years, the use of output from RCMs could be limited when there are some systematic errors in global reanalysis LBC fields [*Frei et al.*, 2003; *Hagemann et al.*, 2004; *Mooney et al.*, 2011; *Teutschbein and Seibert*, 2012]. Systematic biases for the current climate are unavoidable in GCMs/global reanalyses [*Laprise et al.*, 2013; *Fotso-Nguemo et al.*, 2017]. These biases can be propagated through the downscaling process with far

reaching implications on the simulation products and any subsequent applications [*Mehrotra and Sharma*, 2015, 2016]. The first step toward reducing the bias and improving the simulations is to avoid using unrealistic driving boundary conditions. This can be achieved by using the reanalysis with the most accurate LBCs at the intended boundaries of a RCM. *Liang et al*. [2008] advocates for use of regional climate modeling instead of using biased GCM projection of climate changes for impact studies at regional level. As pointed out by *Moalafhi et al*. [2016b], even the reanalysis with the overall most accurate LBCs based on a range of metrics assessed at the boundaries of a RCM, may still contain biases. Regional models thus could be limited in addressing the inherent biases present in GCMs and global reanalyses and hence bias correction may still be required [*Wood et al*., 2004]. Bias correction of reanalyses LBCs prior to dynamical downscaling, for example, ensures that errors are corrected, which would lead to better skill and consistent downscaled products that are independent of the choice of the domain [*Kanamisu and Kanamaru*, 2007]. This downscaling of reanalyses with prior bias-corrected LBC fields offers a relatively cheaper option to a costly high-resolution data assimilation system when high-resolution observations are not available. Combining statistical bias correction with a dynamical downscaling constitutes a hybrid technique that can yield nearly unbiased, high-resolution, physically consistent fields that can be used for climate impact studies [*Colette et al*., 2012]. Recently *Bastola and Misra* [2014] tested products of reanalysis for hydrological application over the US through forcing calibrated hydrological models with five different types of data sets: global reanalyses (National Centers for Environmental Prediction/Department of Energy Reanalysis and European Centre for Medium-Range Weather Forecasts 40-year Reanalysis); dynamically downscaled reanalyses at 10 km grid resolution; stochastically generated data from a weather generator; bias-corrected dynamically downscaled reanalyses; and bias-corrected reanalyses. In that study, the simulated hydrological response to the bias-corrected dynamically downscaled reanalyses data was found to be superior to the other four meteorological data sets over 28 watersheds. The main research question of this study is thus, "Can simple mean and standard deviation bias correction of boundary condition fields of global reanalysis prior to downscaling improve the simulated near-surface temperature and precipitation within a regional domain? Although studies point to superiority of simulated hydrological response of dynamically downscaled reanalyses, little has been done on bias correcting LBCs of the reanalysis before downscaling. This study thus attempts to fill this gap by investigating and demonstrating the impact of dynamically downscaling a bias-corrected reanalyses (ERA-I) on near-surface climate within an example regional domain centered over southern Africa. Ideally, the bias correction would be done on all atmospheric LBCs (temperature, moisture, and winds); however, a spatially continuous wind data set does not currently exist limiting this bias correction to temperature and moisture. How these bias-corrected ERA-I LBCs translate into bias in the near-surface climate in the interior of the domain is explored here.

The rest of the paper is as follows. Methods and data which include WRF setup, observational data sets (including AIRS satellite data), bias correction, and analysis are described in section 2. Results are presented and discussed in sections 3 and 4, respectively, followed by conclusions in section 5.

2. Methods and Data

Three simulations are performed using WRF to downscale the European Centre for Medium range Weather Forecasting Reanalysis ERA-Interim (ERA-I) over a domain centered over southern Africa between 2003 and 2012 all inclusive. The first simulation uses raw ERA-I LBC fields for forcing while the other two use ERA-I with atmospheric temperature and moisture fields bias-corrected using the Atmospheric Infrared Sounder (AIRS) satellite data. The use of ERA-I reanalysis alone here stems from an earlier study where it was found to have a better overall performance compared to Modern Era Retrospective-analysis for Research Applications (MERRA) when downscaled over the same domain using WRF [*Moalafhi et al*., 2016b]. This was after it had been revealed in an earlier study that the two reanalyses provide the most accurate LBCs for downscaling over the same domain [*Moalafhi et al*., 2016a]. Despite this, downscaling ERA-I exhibited bias in precipitation and near-surface temperature.

2.1. WRF Setup

A ten-year regional simulation (2003–2012) is made based on each of the three (3) ERA-I LBCs (one without any bias correction, the second one with mean bias correction, the third one with both the mean and standard deviation bias correction) using the nonhydrostatic Weather Research and Forecasting WRF (ARW)

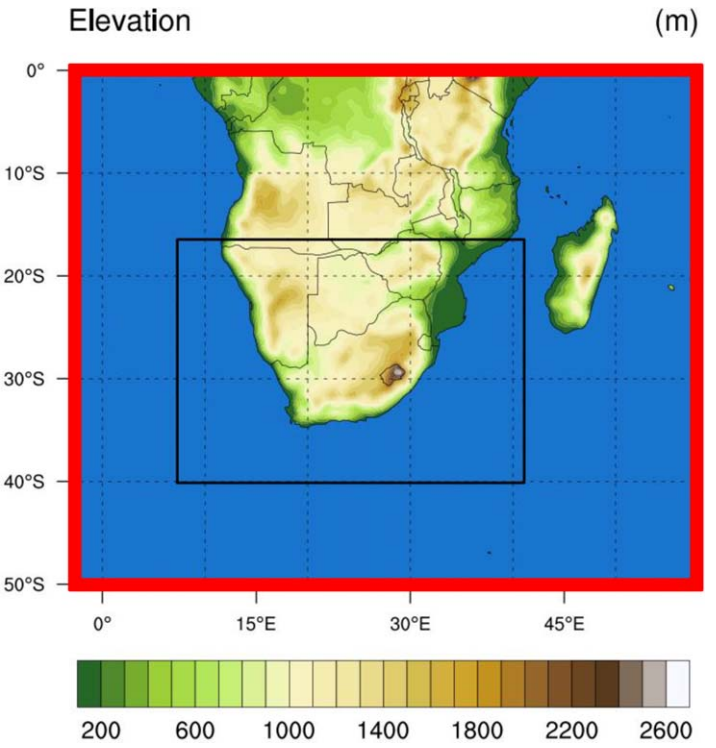

Figure 1. Elevation map for WRF model (m) (full, dx = 50 km), inner (solid black line, dx = 10 km) domain centered over southern Africa also showing locations of boundaries (in red) to the study area.

model, version 3.6 [*Skamarock et al.*, 2008]. The WRF domains setup (Figure 1) is configured so that the inner domain uses a horizontal grid spacing of 10 km, and the outer domain a spacing of 50 km with thirty vertical levels common to both domains. The first year of the model runs is discarded for model spin-up and 10 grid points along the boundary of the inner domain are also left out as the relaxation zone. The WRF was configured to update lateral boundary conditions and sea surface temperature every 6 h using the three reanalysis forcing fields.

Based on efficiency and performance of WRF regional climate simulations especially over southern Africa and Australia [*Crétat et al.*, 2011a, 2011b; *Boulard et al.*, 2012; *Pohl et al.*, 2014; *Ratna et al.*, 2013; *Evans and McCabe*, 2010] the following WRF physical parameterizations were adopted: Single-Moment 5-class microphysics scheme; Rapid Radiative Transfer Model (RRTM) longwave radiation scheme; Dudhia shortwave radiation scheme; Yonsei University planetary boundary layer scheme; Betts-Miller-Janjic cumulus parameterization scheme and Noah land-surface scheme.

2.2. Observational Data Sets

2.2.1. Atmospheric Infrared Sounder (AIRS) Satellite Data

Atmospheric Infrared Sounder (AIRS) satellite data version 6 is used as it provides 4-D global data for both temperature (24 levels) and relative humidity (12 levels). AIRS is the first of a new generation of advanced satellite-based atmospheric sounders that produces daily, high-accuracy, high vertical and horizontal resolution profiles of temperature and water vapor over most of the Earth's surface [*Aumann et al.*, 2003; *Tobin et al.*, 2006; *Susskind et al.*, 2006]. The instrument suite is designed to support climate research and improve weather forecasting with data at 1° × 1° grid resolution and available at http://acdisc.gsfc.nasa.gov/opendap/Aqua_AIRS_Level3/. The data used are level 3 standard products of both descending and ascending overhead passes at 1:30 and 13:30 h local time, respectively, referenced by 0° longitude every day.

The data have high-accuracy retrieval goals of 1 K Root Mean Squared errors in 1 km layers below 100 hPa for air temperature, 10% Root Mean Squared Errors in 2 km layers below 100 hPa for water vapor concentration. Despite these, the large temporal and spatial variability of the atmosphere and difficulties in making accurate measurements of the atmospheric state necessitated continuous careful and detailed validation using well-characterized ground-based sites [*Tobin et al.*, 2006]. In this regard, the continuing efforts to validate and give quality assurance to AIRS products has always been positive [*Fetzer*, 2006; *Divakarla et al.*, 2006]. Among the motivations for increased use of AIRS products is that temperature profile accuracy in the troposphere matches that achieved by radiosondes, and retrievals in both temperature and water vapor are in good agreement with global radiosonde measurements over both land and ocean [*Divakarla et al.*, 2006]. With the latest version (version 6), significant improvement in the ability to obtain both accurate temperature profiles and surface skin temperatures under partial cloud cover conditions has been achieved [*Susskind et al.*, 2014].

2.2.2. Near-Surface Temperature

Two (2) gridded data sets (herein referred to as observations) of monthly near-surface temperature are considered in evaluating performance of the model runs. These are University of Delaware (UD) and the Climate Anomaly Monitoring System (GHCN_CAMS) data sets which are available from NOAA/OAR/ESRL PSD, Boulder, Colorado, USA, from their website at http://www.esrl.noaa.gov/psd/. The observation from the University of Delaware (UD) was developed by compiling together data from a large number of stations both from the Global Historical Climate Network (GHCN2), the Global Synoptic Climatology Network, the Global Summary of the Day (GSOD) from NCDC and the archives of Legates and Willmott monthly and annual station records [*Legates and Willmott*, 1990a, 1990b]. The data set covers the years 1900–2014 at grid resolution of 0.5° × 0.5°. This data set is popular among the research community [*Hao et al*., 2013; *Rawlins et al*., 2012; *Sheffield et al*., 2012]. The other temperature data set, GHCN_CAMS, is a combination of two large individual data sets of station observations collected from the Global Historical Climatology Network version 2 and the Climate Anomaly Monitoring System (GHCN + CAMS). The data set, which is credited for its use of some unique interpolation methods [*Fan and van den Dool*, 2008], is available at 0.5° by 0.5° grid resolutions from 1948 to April 2016.

2.2.3. Precipitation

Precipitation data sets being considered are, University of Delaware (UD), Global Precipitation Climatology Project (GPCP), and Global Historical Climatology Network and The Climate Prediction Center (CPC) Merged Analysis of Precipitation (CMAP). All these data sets are available from NOAA/OAR/ESRL PSD, Boulder, Colorado, USA, from their website at http://www.esrl.noaa.gov/psd/.

The Climate Prediction Center (CPC) Merged Analysis of Precipitation (CMAP) [*Xie and Arkin*, 1997], which has also been investigated over Africa [*Lélé et al*., 2015], is a monthly data set consisting of averaged precipitation rates obtained by merging gauge observations, estimates inferred from a variety of satellite observations, and the NCEP-NCAR reanalysis. The data set is on a 2.5° by 2.5° grid resolution and covers the period from 1979 to April 2016. The GPCP data set is probably the most commonly used data set for global precipitation, including use in climate and hydrology related studies over southern Africa [*Crétat et al*., 2011a, 2011b; *Boulard et al*., 2012; *Pohl et al*., 2014]. The data set is a composite of rain gauge, satellites, and sounding observation data [*Adler et al*., 2003] on a 2.5° by 2.5° grid resolution from 1979 to October 2015. The University of Delaware (UD) precipitation data set, which was compiled similar to the UD temperature, also covers the years 1900–2014 at grid resolution of 0.5° × 0.5°.

These near-surface temperature and precipitation gridded data sets were interpolated to the 0.088° (about 10 km) common grid resolution of the downscaled products (i.e., WRF simulations).

2.3. Bias Correction

Level 3 AIRS satellite data version 6 spanning the years 2003–2012 is available globally at 1° × 1° grid resolution. Both the descending (1:30 A.M.) and ascending (1:30 P.M.) overpass times are combined in this study to produce time series of temperature and relative humidity every 12 h. These fields are interpolated to 6 hourly, 0.72° × 0.72° grid resolution and to the same pressure levels (38) of ERA-I reanalysis which is being bias-corrected and subsequently used as initial and lateral boundary condition forcing fields for downscaling. AIRS temperature is over 24 pressure levels (1000–1 hPa) and 12 levels for relative humidity (1000–100 hPa). *Teutschbein and Seibert* [2012] demonstrated the viability of different bias correction approaches using an ensemble of eleven different RCM-simulated temperature and precipitation and subsequent impacts on hydrological simulations. In the study, most methods were able to correct daily mean values but power transformation or distribution mapping were also capable of correcting other statistical properties. Despite the common use of scaling or quantile mapping bias correction approaches, these are often found to overlook biases in persistence related attributes like time dependence in raw GCM simulations of rainfall and other climate variables [*Lin*, 2007; *Bates et al*., 2008; *Mehrotra and Sharma*, 2015]. In this study mean and standard deviation bias corrections are made to atmospheric temperature and relative humidity. More sophisticated bias correction methods quickly lead to substantial computational cost when correcting 4-D fields. This initial effort demonstrates the implementation of objectively chosen reanalysis downscaling with prior bias-corrected LBC fields. The study, the first of its kind, attempts to determine the impact of this downscaling of the most accurate reanalysis with prior bias correction on temperature and precipitation within the regional domain centered over southern Africa. The first bias correction focuses on biases in the mean for each variable at each grid location, and

the second uses both mean and standard deviation in the same setting. The bias correction [*Mehrotra and Sharma*, 2012, 2015] is implemented at daily time scale on the 6 hourly data in which each of the ERA-I fields (atmospheric temperature and relative humidity) is transformed toward the AIRS mean (μ_A) using the transformation

$$X'_R = X_R - \mu_R + \mu_A, \tag{1}$$

where X'_R is the transformed ERA-I data, X_R is original ERA-I data, μ_R and μ_A are means of original ERA-I and AIRS, respectively.

When the bias correction is extended to also include standard deviation, the ERA-I data is recentered and rescaled using

$$X''_R = S_A\left(X_R - \mu'_R\right)/S_R + \mu'_R, \tag{2}$$

where S_A and S_R are standard deviation of AIRS and ERA-I, respectively, μ'_R is mean of the mean transformed ERA-I.

To assess the influence of the bias correction at the 6 hourly time scale of the LBC fields, mean bias is computed between the corrected ERA-I and AIRS fields alongside that between raw ERA-I and AIRS at the boundary panels of the domain. The panels are located at the boundaries of the RCM domain, stretching inward by 4°. The resultant panels of the domain were thus demarcated as north (–3°E to 58°E, −2°S to 1°S), south (–3°E to 58°E, −50°S to −47°S), east (55°E–58°E, −47°S to −2°S), and west (–3°E to 0°E, −47°S to −2°S).

2.4. Analysis

2.4.1. LBC Fields

Impact of the LBC fields daily correction on the 6-hourly fields is investigated through computing mean bias over the individual boundary panels. The errors are then displayed through vertical contour plots and also summarized in a table to aid in the investigations.

Mean bias is given as

$$\overline{R} - \overline{Obs}, \tag{3}$$

where $\overline{R}$ is ERA-I reanalysis averaged temperature or relative humidity, either raw or corrected, and $\overline{Obs}$ is averaged AIRS temperature or relative humidity.

2.4.2. Models Simulations

Temperature and precipitation simulated by the models are evaluated against the gridded observations based on mean bias, RMSE, and temporal correlation. These are done both annually and seasonally. Observational Range Adjusted (ORA) computation of error statistics is adopted to evaluate the model performance against all observational data sets collectively [*Evans et al.*, 2015]. This approach takes into consideration uncertainties among the different gridded observations considered in which the model is considered to have no error when it falls within the range of the observational data sets. When the model is outside this range the error is the difference between the model and the nearest observation. This is achieved by creating a pseudo-observational time series which equals the model value when the model falls within the observational range, and takes the maximum or minimum observation value when the model falls above or below the observational range, respectively. The pseudo-observation series, Obs_{ORA}, can be represented by

$$\begin{aligned} Obs_{ORA} &= Model \ \text{ if } \ Obs_{\min} \le Model \le Obs_{\max}, \\ Obs_{ORA} &= Obs_{\min} \ \text{ if } \ Model < Obs_{\min}, \\ Obs_{ORA} &= Obs_{\max} \ \text{ if } \ Model > Obs_{\max}, \end{aligned} \tag{4}$$

where Obs_{ORA} is the Observational Adjusted Range (ORA) value, $Obs_{\min}$ is the minimum value from all the observations, $Obs_{\max}$ is the maximum value from all the observations, and *Model* is the model value.

The ORA-adjusted values are subsequently used in computations of error statistics. The differences of the means between the model and the ORA pseudo-observation series is given by mean bias as

$$\overline{M}-\overline{Obs}_{ORA}, \tag{5}$$

where $\overline{M}$ is model-averaged temperature or precipitation and $\overline{Obs}_{ORA}$ is averaged observed temperature or precipitation.

The RMSE is calculated as

$$RMSE=\sqrt{\frac{1}{n}\left(\sum_{i=1}^{n}\left(M_i-Obs_{ORAi}\right)^2\right)}, \tag{6}$$

where n is the number of time steps and Obs_{ORAi} and M_i are the observations and model product values, respectively, for time i = 1,. . .,n.

Temporal correlation coefficient is used to evaluate the goodness of fit by performing linear regression between observational range adjusted (ORA) and models' temperature or precipitation.

$$r=\frac{\sum_{i=1}^{n}\left(Obs_{ORA_i}-\overline{Obs}_{ORA}\right)\left(M_i-\overline{M}\right)}{\sqrt{\sum_{i}^{n}\left(Obs_{ORA_i}-\overline{Obs}_{ORA}\right)^2}\sqrt{\sum_{i}^{n}\left(M_i-\overline{M}\right)^2}}, \tag{7}$$

where $\overline{Obs}_{ORA}$ and $\overline{M}$ are observational range adjusted (ORA) and model mean values, respectively.

3. Results

3.1. Bias Correction

Bias correction is aided through a summary table of mean bias over the individual boundary panels and vertical contour plots of the errors considering midtroposphere to the surface (i.e., 500–1000 hPa levels). Vertical contour plots of mean bias between raw ERA-I and AIRS reveals how over a panel and over the atmospheric levels the reanalysis compares to AIRS. The aim of bias correction is to bring reanalysis as close as possible to AIRS and thus vertical contour plots of mean bias between corrected ERA-I and AIRS should be as close as possible to zero over the individual panels and over levels of the atmosphere. Overall impact of bias correction for a panel is assessed through averaging mean bias over the panel and over the levels of the atmosphere. The resultant panels of the domain are; north (–3°E to 58°E, −2°S to 1°S), south (–3°E to 58°E, −50°S to −47°S), east (55°E–58°E, −47°S to −2°S), and west (–3°E to 0°E, −47°S to −2°S).

3.1.1. Temperature

Mean bias over the individual boundary panels and over the levels show that raw ERA-I reanalysis is warm-biased (overestimates temperature) over the boundary panels except the northern one (Table 1). The northern boundary panel has the largest bias by raw ERA-I (–0.37 K), with western panel coming a distant second with mean bias of 0.14 K. Mean bias over the panels based on both the mean correction (MeanCorr-AIRS) and the mean and standard deviation correction (M&SDCorr-AIRS) are similar. Mean and standard deviation correction is, however, superior for the southern and eastern panels with the bias reduced to zero. In both corrections, the cold bias of the northern panel is reduced considerably (i.e., from −0.37 K using raw ERA-I to −0.03 K using corrected ERA-I).

Vertical contours of mean bias reveal that Raw ERA-I is particularly warm-biased toward high latitudes around 800 hPa over the eastern boundary panel (Figure 2). Over the western and southern boundary panels, this warm bias around 800 hPa pressure level is especially visible toward the low latitudes and larger over the former (Figures 2 and 3). Raw ERA-I also shows largest cold bias especially toward the surface over the northern and southern boundary panels. As also revealed through Table 1, bias using both corrections are very similar to each other.

3.1.2. Relative Humidity

Raw ERA-I is wet-biased (overestimates relative humidity) over all the boundary panels (Table 1). The northern boundary panel has the largest bias (4.63%) followed by the southern boundary panel (1.44%). Although the bias slightly varies between the two corrections, the corrections are closer to each other. Mean and standard deviation correction is superior except over the northern panel. The largest bias correction is over the northern panel, which is the only one that yields dry bias after the corrections.

Table 1. Temperature (K) and Precipitation (mm) Mean Bias Between Corrected ERA-I and AIRS, also Showing That Between Raw ERA-I and AIRS at the Respective Boundaries of the Domain

	Temperature Mean Bias (K)			Relative Humidity Mean Bias (%)		
	MeanCorr-AIRS	M&SDCorr-AIRS	Raw-AIRS	MeanCorr-AIRS	M&SDCorr-AIRS	Raw-AIRS
N	−0.03	−0.03	−0.37	0.24	0.27	4.63
S	0.01	0.00	0.02	−0.76	−0.73	1.44
E	0.01	0.00	0.01	−0.33	−0.28	0.69
W	0.05	0.05	0.14	−0.40	−0.35	0.77

For both the eastern and western boundary panels, raw ERA-I is wet biased over the lower layers of the atmosphere (Figure 4). This wet bias is larger over the western boundary panel, especially toward low latitudes. Raw ERA-I shows largest wet bias at upper layers and lower layers over the northern boundary panel (Figure 5). For the southern boundary panel, the largest wet bias is a thing horizontal band around 950 hPa. There is also large bias around 500 hPa. All these bias have been minimized during the corrections.

3.2. Models Mean Bias (Model Observations)

3.2.1. Temperature

University of Delaware (UD) and Global Historical Climatology Network version 2 and the Climate Anomaly Monitoring System (GHCN_CAMS) are used as temperature observational data sets for evaluating the models performance. The WRF run using raw ERA-I forcing (WRF_ERA-Iraw) is only warm-biased in summer (DJF) and spring (SON) as could be seen in Table 2. The largest bias is during winter (JJA) at −0.44 K. Transition seasons (MAM, SON) show best performances by WRF_ERA-Iraw.

Annually, WRF_ERA-Iraw is generally cold biased over the study area despite the anomalous warm bias over the Namibian coastal plain (Figure 6a). Seasonally, the anomalous warm bias over the Namibian coastal plain is still visible (Figure 7a). Winter's largest cold bias among the seasons is evident particularly to the east over southern Mozambique and over northern to central parts of the domain covering northern Botswana and northwestern Namibia (Figure 7a).

WRF forced with both mean bias-corrected ERA-I (WRF_ERA-IcorrM) and mean and standard deviation bias-corrected ERA-I (WRF_ERA-IcorrM&SD) atmospheric temperature is warm biased annually and over all seasons (Table 2). In both cases, the bias improvement is only in winter (JJA). Contrary to WRF forced by ERA-Iraw, where least bias is in spring (SON), the season shows the largest biases from WRF forced by the bias-corrected atmospheric temperature. WRF_ERA-IcorrM&SD is superior to WRF_ERA-IcorrM except during summer (DJF). The anomalous warm bias over the Namibian coastal plain appears a bit worse in WRF_ERA-IcorrM and WRF_ERA-IcorrM&SD especially the northern part as is seen in the annual near-surface temperature contour plots over the domain (Figure 6). This could partly be attributed to the significant reduction in cold bias during the bias correction prior to downscaling at the northern boundary (Table 1). Despite the bias correction at best marginally reducing the atmospheric temperature biases at the western, southern, and eastern boundaries prior to downscaling, the model forced by the bias-corrected atmospheric temperature generally increases near-surface temperature over the domain. Seasonally, the anomalous warm bias over the western coastal plain is more evident during autumn (MAM) from all three model run simulations (Figure 7). Simulations based on bias-corrected LBCs show more warm bias in spring (SON) and winter (JJA) especially over most of South Africa. Both WRF_ERA-IcorrM and WRF_ERA-IcorrM&SD show less cold bias over Mozambique, northern Botswana, and northeastern Namibia than that which is clearly shown by WRF_ERA-Iraw during winter (Figure 7).

3.2.2. Precipitation

The global gridded precipitation data sets considered as observations are University of Delaware (UD), Global Precipitation Climatology Project (GPCP), and The Climate Prediction Center Merged Analysis of Precipitation (CMAP). The models performances are thus evaluated against the three data sets collectively. WRF_ERA-Iraw is found to be dry biased annually and over all the seasons except in spring (MAM) (Table 2). The largest bias over the seasons are during spring (–17.86 mm) followed by autumn (17.04 mm).

The eastern part of the domain falling over Mozambique has the largest annual dry bias (Figure 8a). Northern to central Botswana and northern Namibia are the other areas with notable dry bias by WRF_ERA-Iraw. To the south east of the domain over the Drakensburg and Lesotho areas, WRF_ERA-Iraw shows the largest

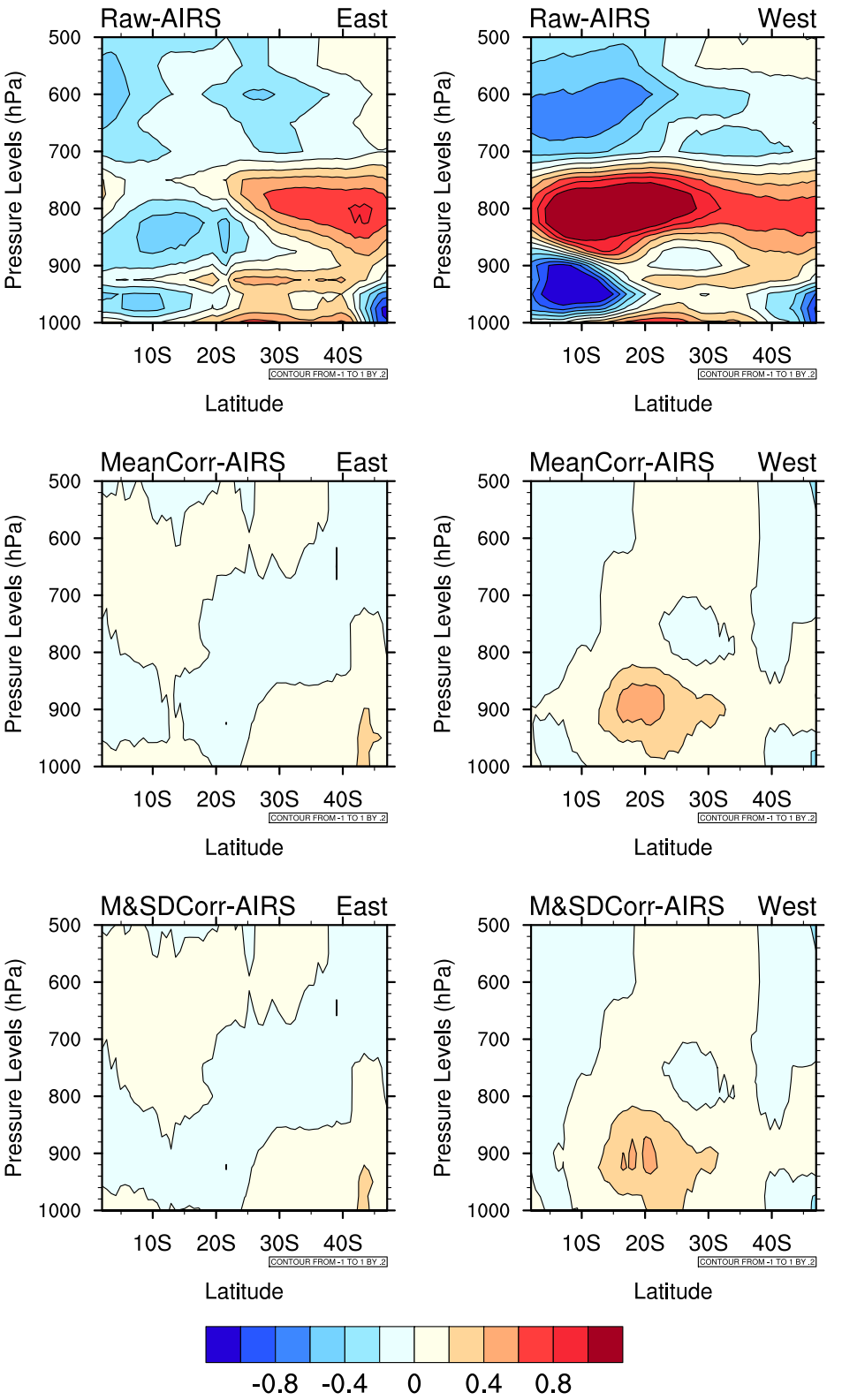

Figure 2. Vertical contour plots of temperature (K) mean bias between raw ERA-I and AIRS (Raw-AIRS), mean corrected ERA-I and AIRS (MeanCorr-AIRS) and mean and standard deviation corrected ERA-I and AIRS (M&SDCorr-AIRS) at the eastern and western boundaries of the domain.

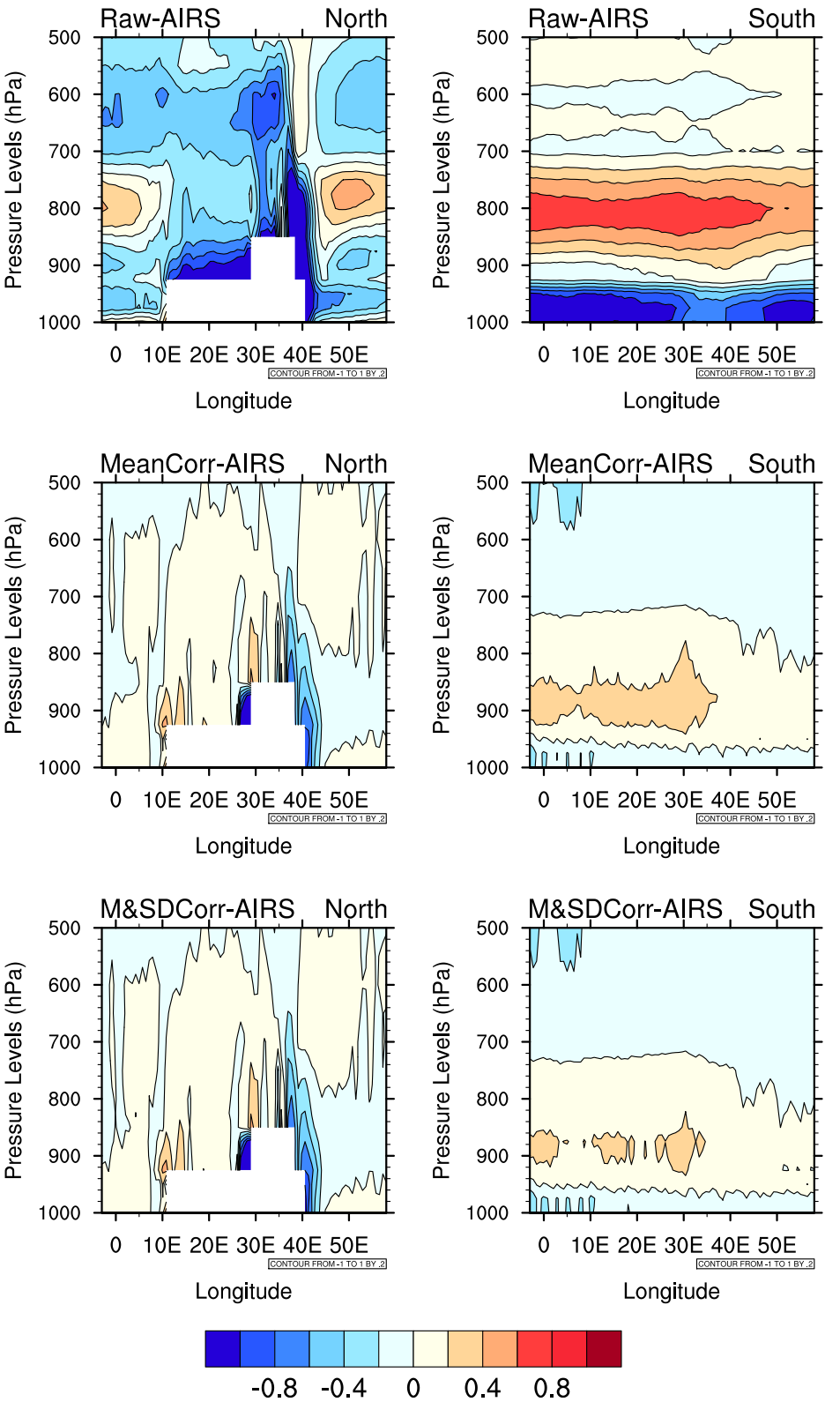

Figure 3. Vertical contour plots of temperature (K) mean bias between raw ERA-I and AIRS (Raw-AIRS), mean corrected ERA-I and AIRS (MeanCorr-AIRS) and mean and standard deviation corrected ERA-I and AIRS (M&SDCorr-AIRS) at the northern and southern boundaries of the domain.

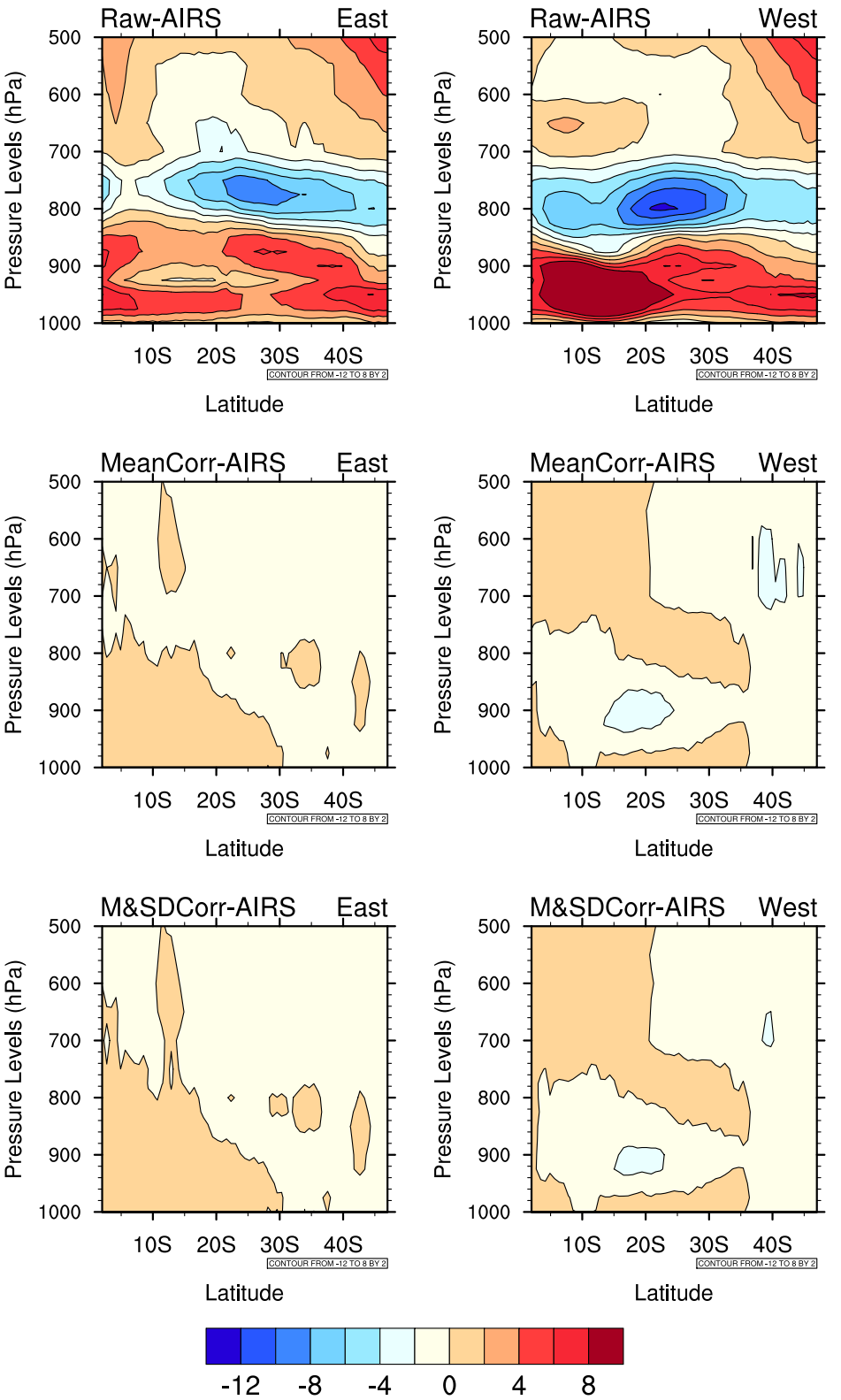

Figure 4. Vertical contour plots of relative humidity (%) mean bias between raw ERA-I and AIRS (Raw-AIRS), mean corrected ERA-I and AIRS (MeanCorr-AIRS) and mean and standard deviation corrected ERA-I and AIRS (M&SDCorr-AIRS) at the eastern and western boundaries of the domain.

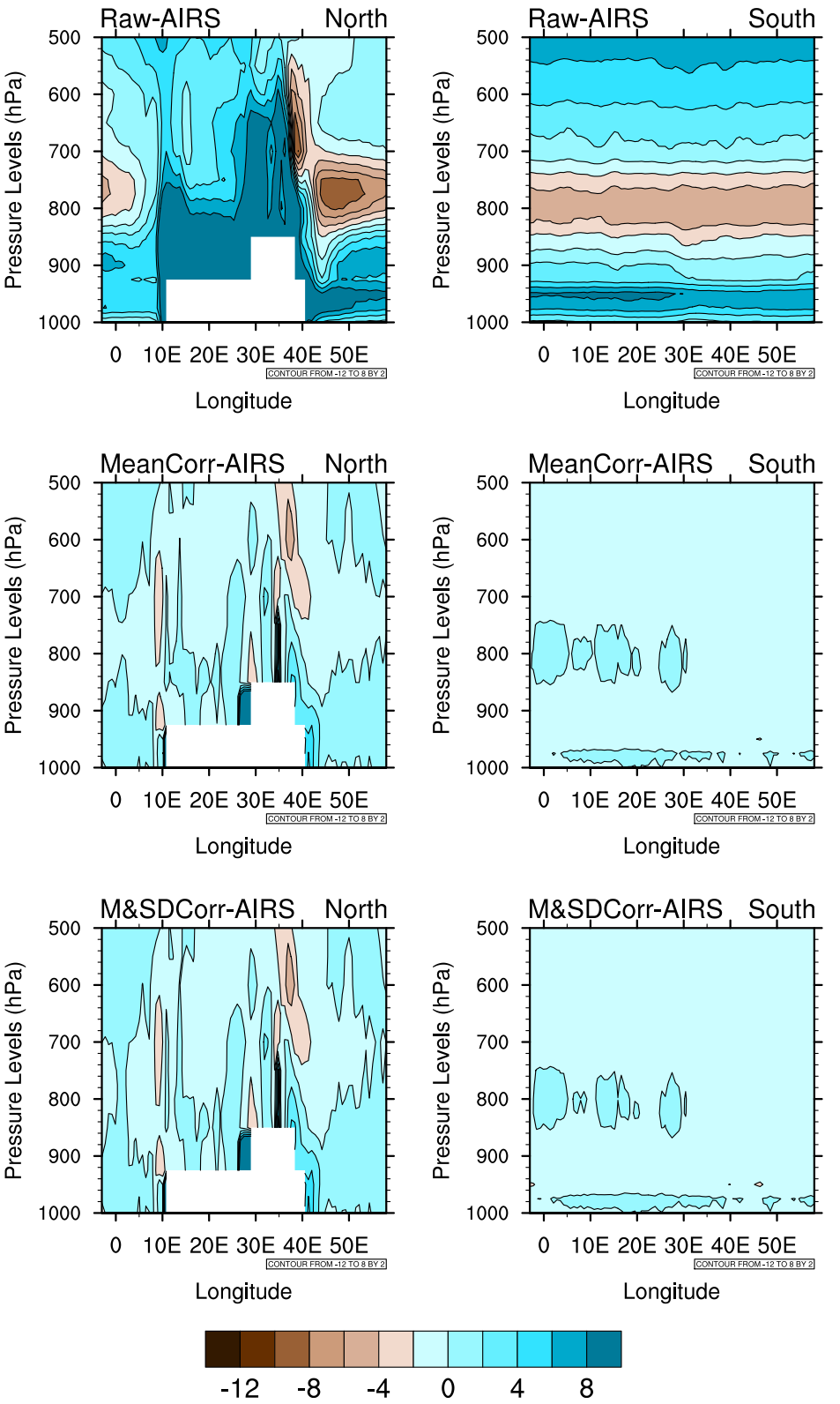

Figure 5. Vertical contour plots of relative humidity (%) mean bias between raw ERA-I and AIRS (Raw-AIRS), mean corrected ERA-I, and AIRS (MeanCorr-AIRS) and mean and standard deviation corrected ERA-I and AIRS (M&SDCorr-AIRS) at the northern and southern boundaries of the domain.

Table 2. Observational Range Adjusted (ORA) Mean Bias of Annual and Seasonal Temperature (K) and Precipitation (mm) for the Whole Study Period (2004–2012)

	Temperature (K) Bias			Precipitation (mm) Bias		
Timescale	WRF_ERA-Iraw	WRF_ERA-IcorrM	WRF_ERA-IcorrM&SD	WRF_ERA-Iraw	WRF_ERA-IcorrM	WRF_ERA-IcorrM&SD
DJF	0.18	0.37	0.40	−11.95	19.54	0.07
MAM	−0.09	0.43	0.42	17.04	15.47	15.58
JJA	−0.44	0.32	0.25	−2.20	−3.89	−4.78
SON	0.04	0.67	0.59	−17.86	−12.68	14.54
Annual	−0.17	0.38	0.32	−6.38	9.78	1.77

wet bias due to the model's struggle in handling orographic forcing. The bias patterns are also revealed at seasonal scales (Figure 9a). The wettest season (summer) shows the largest bias in both magnitude and spatial extent. The eastern part over Mozambique, north to central Botswana in the center of the domain, and mostly northwestern Namibia have notable dry bias. The southeastern part over the Drakensburg and Lesotho areas show largest wet bias by WRF_ERA-Iraw.

Precipitation bias are generally improved in WRF_ERA-IcorrM&SD, especially during summer (0.07 mm for WRF_ERA-IcorrM&SD, −11.95 mm for WRF_ERA-Iraw) and annually (1.77 mm for WRF_ERA-IcorrM&SD, −6.38 mm for WRF_ERA-Iraw) as summarized in Table 2. WRF_ERA-IcorrM shows reversals of dry bias from WRF_ERA-Iraw during summer (19.54 mm for WRF_ERA-IcorrM&SD, −11.95 mm for WRF_ERA-Iraw) and annually (9.78 mm for WRF_ERA-IcorrM&SD, −6.38 mm for WRF_ERA-Iraw). Dry bias of annual precipitation over the domain is generally reduced in both WRF_ERA-IcorrM and WRF_ERA-IcorrM&SD (Figure 8). In both cases, there is increased precipitation biases over Mozambique, and northern to central Botswana (Figure 8). WRF_ERA-IcorrM also shows increased precipitation bias over central Zimbabwe. The increase in spatial extent of precipitation bias is also noticed around the high elevation areas of the Drakensburg in South Africa. These are also reflected over the seasons (Figure 9).

3.3. Models Root Mean Squared Error (RMSE)

For temperature, WRF_ERA-Iraw performs best annually and during summer (Table 3). Similar to mean bias, largest RMSE is evident over the Namibian coastal plain (Figure 10a). Despite this, WRF_ERA-Iraw's performance is fairly uniform over the domain. Considering precipitation, WRF_ERA-Iraw is superior during winter (JJA) while summer (DJF) has the worst performance among the seasons, only better than annual (Table 3). WRF_ERA-Iraw performs best over the southwestern part of the domain bordering Namibia, Botswana, and South Africa (Figure 11a). Another notable improved performance is to the east, spreading slightly either side of the borders between Botswana, Zimbabwe, South Africa and into Mozambique.

Both WRF_ERA-IcorrM and WRF_ERA-IcorrM&SD are superior to WRF_ERA-Iraw in near-surface temperature simulations (Figure 10 and Table 3). WRF_ERA-IcorrM&SD is better than WRF_ERA_IcorrM. Like for WRF_ERA-Iraw, best performances are during summer for both bias-corrected model simulations. For precipitation, both bias-corrected model simulations are only slightly superior to WRF_ERA-Iraw during spring

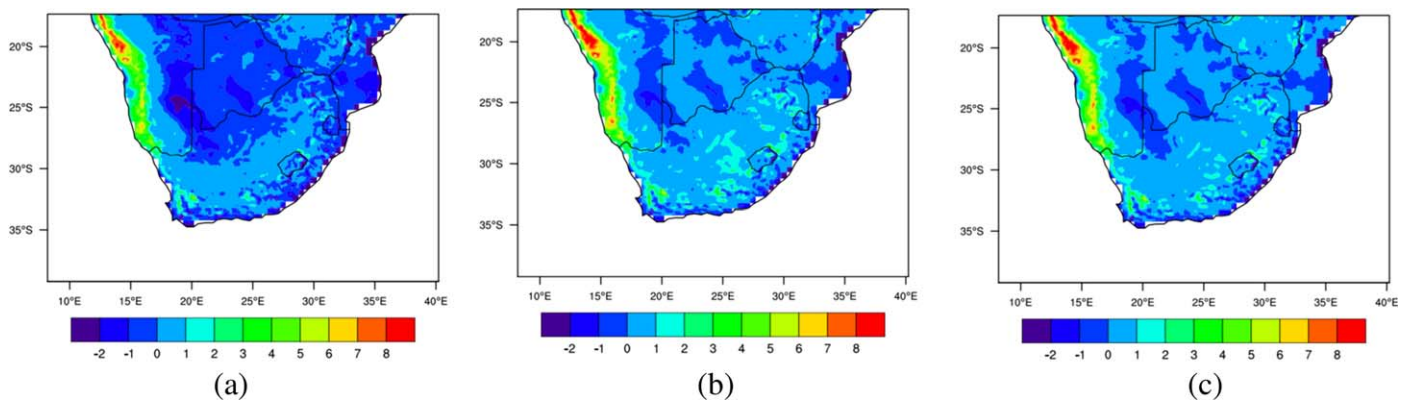

Figure 6. Observational Range Adjusted (ORA) mean bias (model-observations) of annual surface temperature (K) for (a) WRF_ERA-Iraw, (b) WRF_ERA-IcorrM, and (c) WRF_ERA-IcorrMSD.

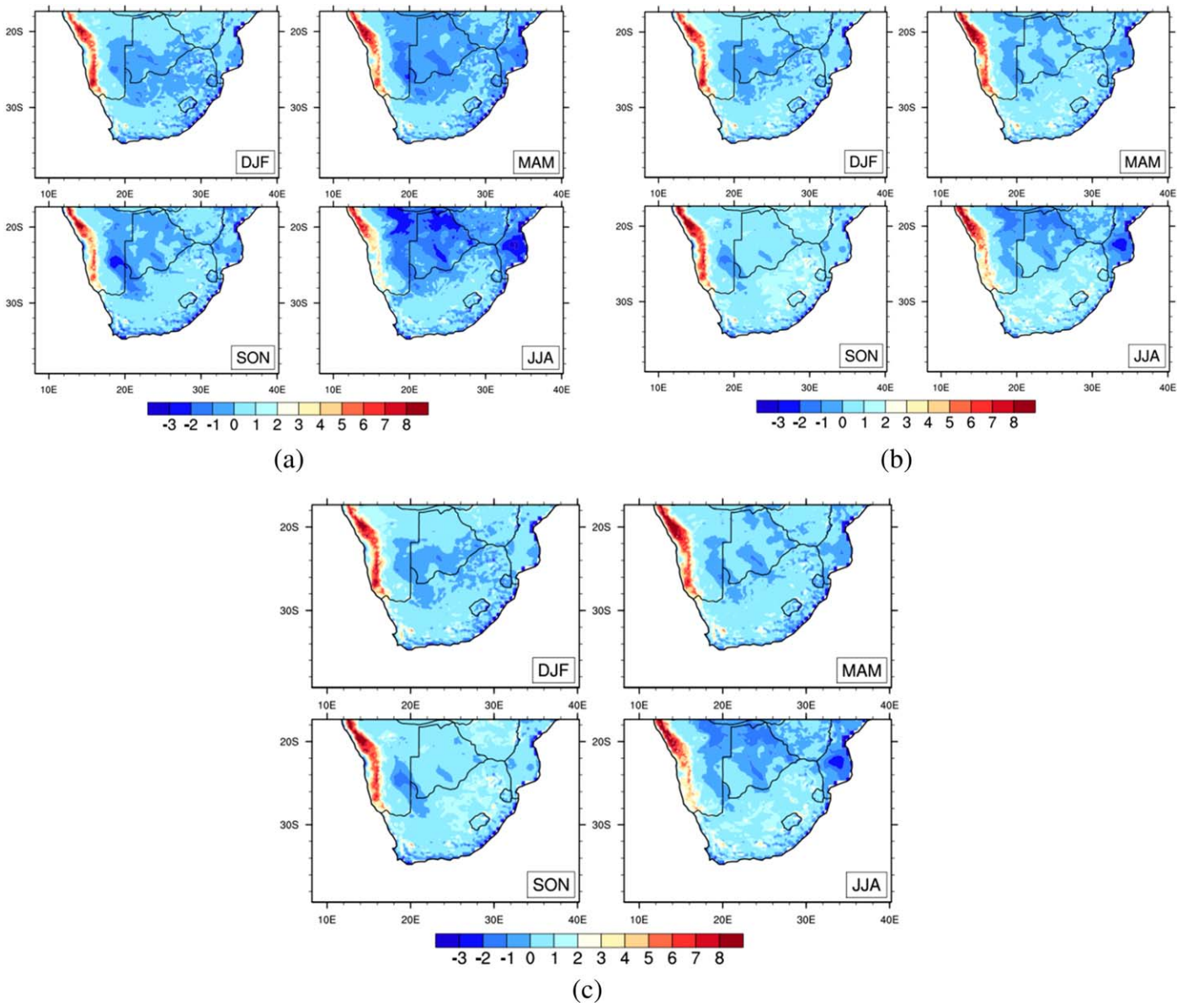

Figure 7. Seasonal Temperature (K) Observational Range Adjusted (ORA) mean bias for (a) WRF_ERA-Iraw, (b) WRF_ERA-IcorrM, and (c) WRF_ERA-IcorrM&SD.

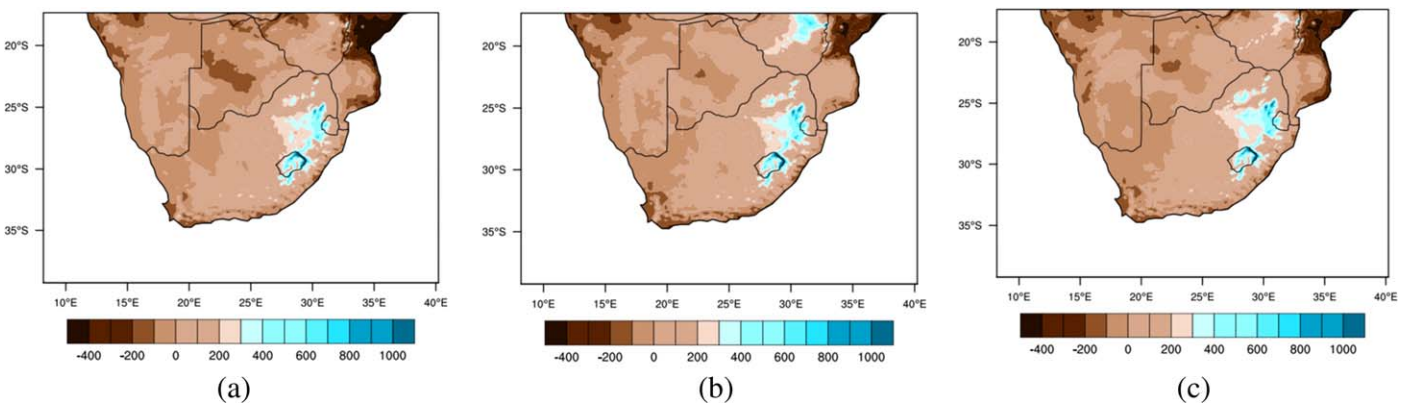

Figure 8. Observational Range Adjusted (ORA) mean bias (model-observations) of annual precipitation (mm) for (a) WRF_ERA-Iraw, (b) WRF_ERA-IcorrM, and (c) WRF_ERA-IcorrMSD.

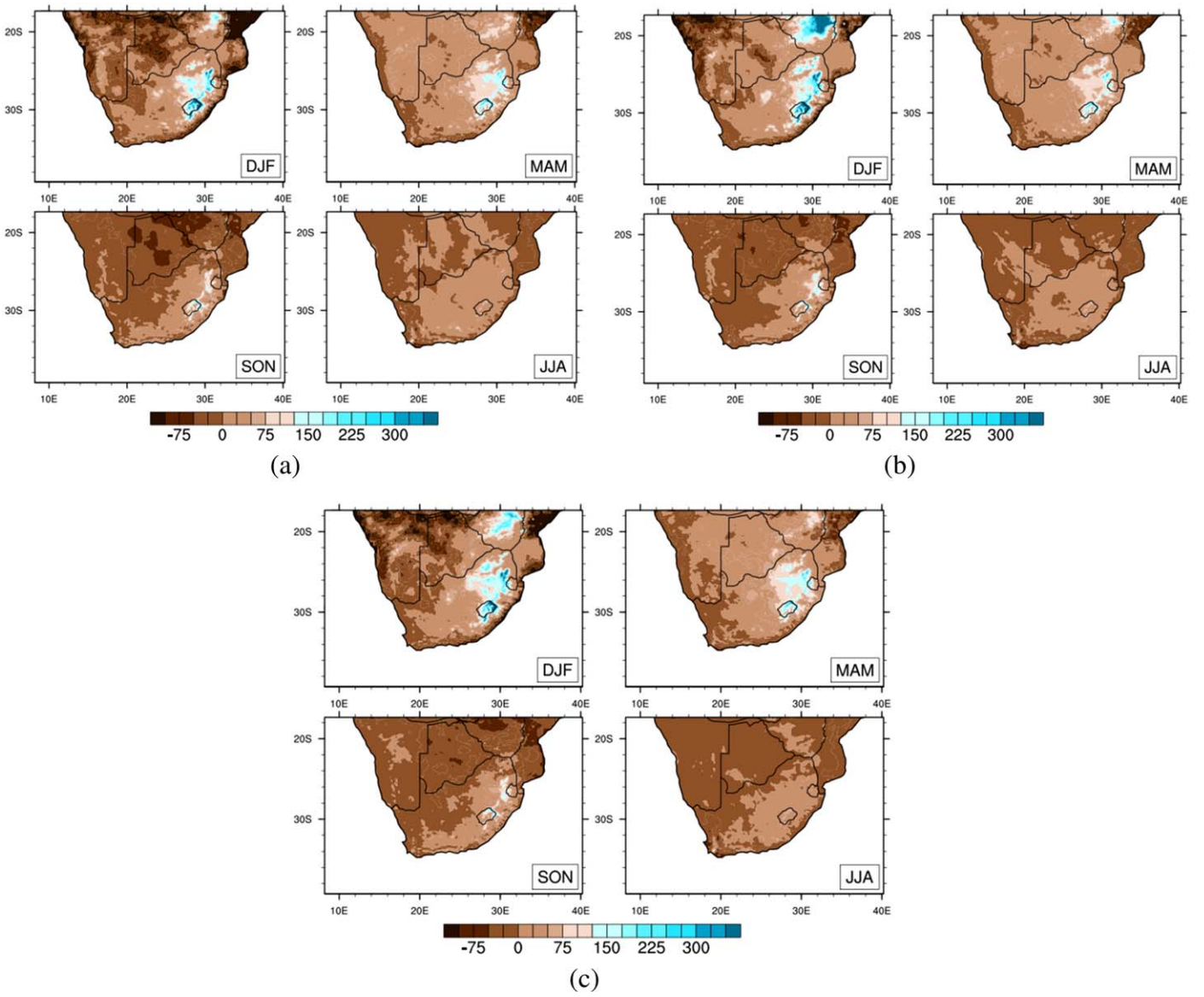

Figure 9. Seasonal Precipitation (mm) Observational Range Adjusted (ORA) mean bias for (a) WRF_ERA-Iraw, (b) WRF_ERA-IcorrM, and (c) WRF_ERA-IcorrM&SD.

(SON) and winter (JJA) as shown in Table 3. Here WRF_ERA-IcorrM&SD is marginally better than WRF_ERA-IcorrM in precipitation RMSE. Annually, RMSE based on bias-corrected model simulations are similar to those based on WRF_ERA-Iraw but with the former performances worse over northwestern Namibia (Figure 11). WRF_ERA-IcorrM&SD also perform worse over western Botswana.

Table 3. Observational Range Adjusted (ORA) Mean RMSE of Annual and Seasonal Temperature (K) and Precipitation (mm) for the Whole Study Period (2004–2012)

	Temperature (K) RMSE			Precipitation (mm) RMSE		
Timescale	WRF_ERA-Iraw	WRF_ERA-IcorrM	WRF_ERA-IcorrM&SD	WRF_ERA-Iraw	WRF_ERA-IcorrM	WRF_ERA-IcorrM&SD
DJF	1.94	1.00	1.02	96.63	104.77	105.42
MAM	2.23	1.29	1.26	58.88	65.92	64.74
JJA	2.22	1.33	1.29	19.83	17.38	17.08
SON	2.12	1.13	1.11	40.57	37.59	37.35
Annual	1.92	0.92	0.91	132.33	143.72	151.23

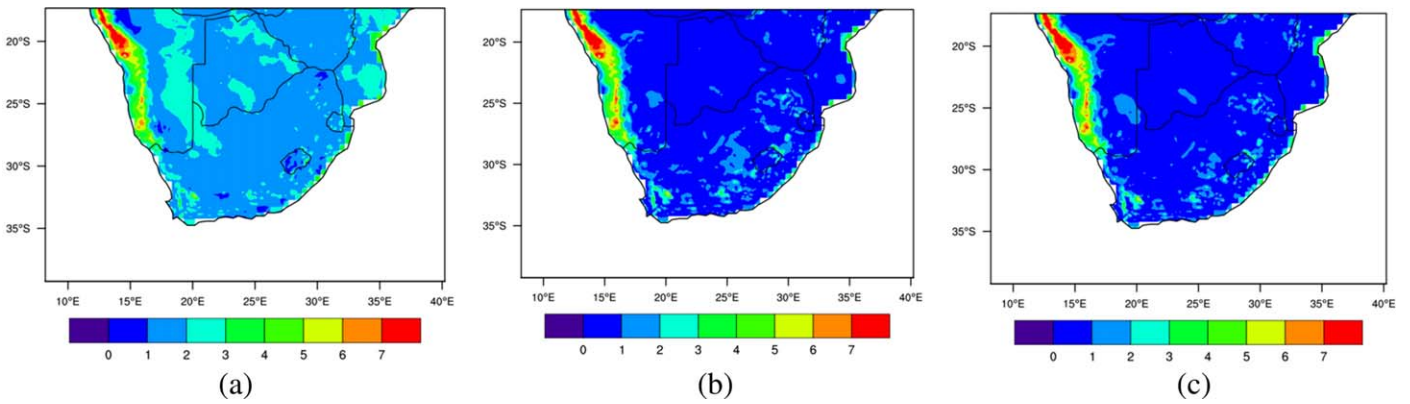

Figure 10. Observational Range Adjusted (ORA) RMSE of annual surface temperature (K) for (a) WRF_ERA-Iraw, (b) WRF_ERA-IcorrM, and (c) WRF_ERA-IcorrMSD.

3.4. Models Temporal Correlation

Temporal correlation between WRF_ERA-Iraw and observations is poor for both temperature and precipitation (Table 4). For temperature, the best correlation is during summer (DJF) and spring (SON) at 0.35. Autumn (MAM) has the poorest correlation. WRF_ERA-Iraw is poorly correlated, mostly negative, along the coastal line and over the center of the domain extending between western Botswana and eastern Namibia (Figure 12a). Based on Table 4, WRF_ERA-Iraw's precipitation is better correlated with observed precipitation during autumn (MAM) and annually. Poorest correlation is during winter (JJA). The northeastern part over Mozambique and western to central Namibia show the poorest and mostly negative correlation (Figure 13a).

Temporal correlations in near-surface temperature are generally improved in bias-corrected model simulations with WRF_ERA-IcorrM marginally better than WRF_ERA-IcorrM&SD (Table 4). In the three cases, best correlations are during summer (DJF) and spring (SON). Considering precipitation, correlations in WRF_ERA-IcorrM are marginally better than in WRF_ERA-IcorrM&SD (Table 4). Similar to WRF_ERA-Iraw, worst correlations are in winter (JJA) for both bias-corrected model runs. Annually, WRF_ERA-IcorrM&SD shows the largest negative correlation over the center of the domain, which is not present in WRF_ERA-IcorrM and WRF_ERA-Iraw (Figure 13).

4. Discussions

Daily bias correction of atmospheric temperature and moisture (relative humidity) brings about the desired impact on the 6 hourly fields as assessed through the boundary panels of the domain from midtroposphere to the surface (i.e., 500–1000 hPa). Although the bias corrections have similar impact, mean and standard deviation is superior for both atmospheric temperature and relative humidity.

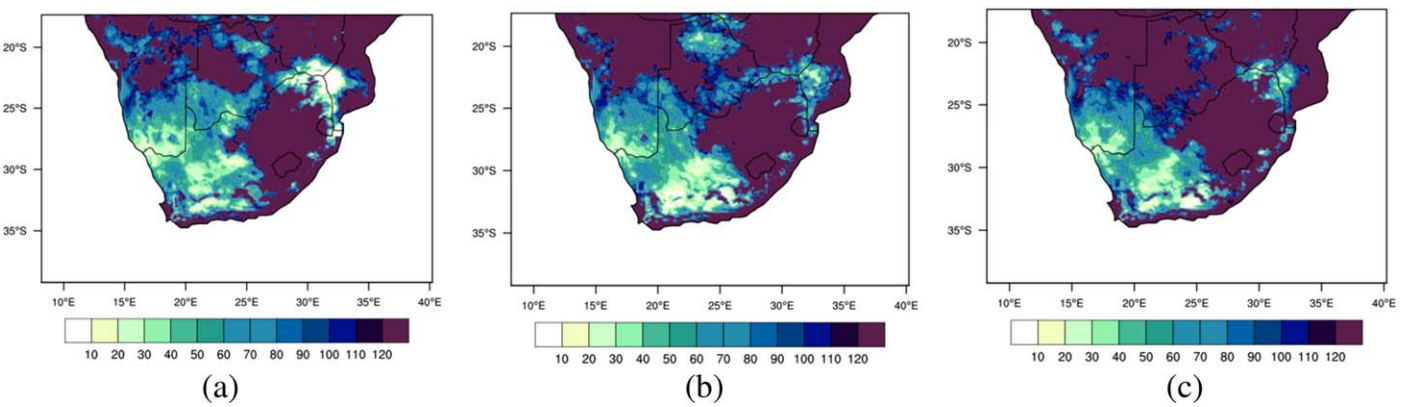

Figure 11. Observational Range Adjusted (ORA) RMSE of annual precipitation (mm) for (a) WRF_ERA-Iraw, (b) WRF_ERA-IcorrM, and (c) WRF_ERA-IcorrMSD.

Table 4. Observational Range Adjusted (ORA) Mean Temporal Correlation of Annual and Seasonal Temperature (K) and Precipitation (mm) for the Whole Study Period (2004–2012)

	Temperature (K) Temporal Correlation			Precipitation (mm) Temporal Correlation		
Timescale	WRF_ERA-Iraw	WRF_ERA-IcorrM	WRF_ERA-IcorrM&SD	WRF_ERA-Iraw	WRF_ERA-IcorrM	WRF_ERA-IcorrM&SD
DJF	0.35	0.42	0.47	0.28	0.35	0.34
MAM	0.06	0.34	0.28	0.50	0.27	0.24
JJA	0.26	0.19	0.17	0.20	0.29	0.22
SON	0.35	0.42	0.45	0.32	0.31	0.35
Annual	0.25	0.40	0.32	0.44	0.46	0.30

Despite the bias correction of atmospheric temperature and relative humidity being impactful on the driving LBCs prior to the downscaling, the impact on the resultant simulations gives mixed results which implies that maybe different types of bias correction strategies (such as the more complex alternatives that maintain intervariable relationships as per *Mehrotra and Sharma* [2015]) should be considered instead of the approaches considered here. It might also be that an altered configuration of WRF model that is more amenable to the influence of the lateral and lower boundaries should be adopted for this domain. Lack of wind LBCs correction cannot be ruled out as another limiting factor that might have impacted the simulations. It is interesting that bias correction of the LBCs has led to cooler (except the northern boundary) and drier boundary conditions on average, but this has translated into a generally warmer and wetter land surface. The vertical structure of the LBC bias correction plays an important role here. Most of the temperature decreases imposed through the bias correction are occurring around 800 hPa elevation, while the near-surface layers are often warming. Meanwhile, most of the humidity decreases are occurring near the surface while increases are occurring around 800 hPa elevation.

This means that around 800 hPa, near the top of the daytime planetary boundary layer, the atmosphere entering the domain is closer to saturation. Meanwhile, surface layer air masses entering from the west or east are warmer and drier. These surface air masses must travel over significant ocean distances before reaching land and while doing so readily evaporate more water than the control simulation. The net effect of these processes is an increase in the total precipitable water in air masses reaching the land. This in turn leads to precipitation events generally producing higher rainfall totals. Since the number of precipitation events does not change, this leads to higher total precipitation over land.

It is also observed that simulations with prior bias correction of LBCs show similarities to those without any prior correction of LBCs especially in regard to anomalous high temperature over the Namibian coastal plain and notable wet bias over high altitude areas (and also dry bias over Mozambique). The temperature anomaly over the Namibian coastal plain was also revealed in a study by *Moalafhi et al*. [2016b] using the same WRF configuration to downscale ERA-I and MERRA over the domain. In that study, *Moalafhi et al*. [2016b] attributed this anomalous warm bias to low level air masses that cool over the *Benguela* current not crossing onto the coastal plain frequently enough, and air masses descending from the inland plateau onto the coastal plain warming the low-level air too much. This anomaly was also revealed in other past studies over

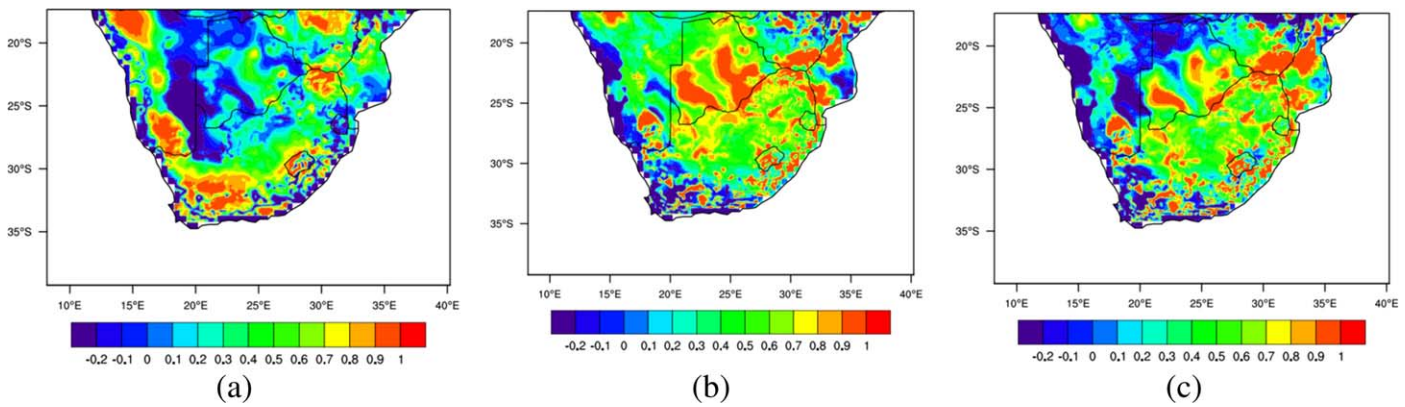

Figure 12. Observational Range Adjusted (ORA) temporal correlation of annual surface temperature (K) for (a) WRF_ERA-Iraw, (b) WRF_ERA-IcorrM, and (c) WRF_ERA-IcorrMSD.

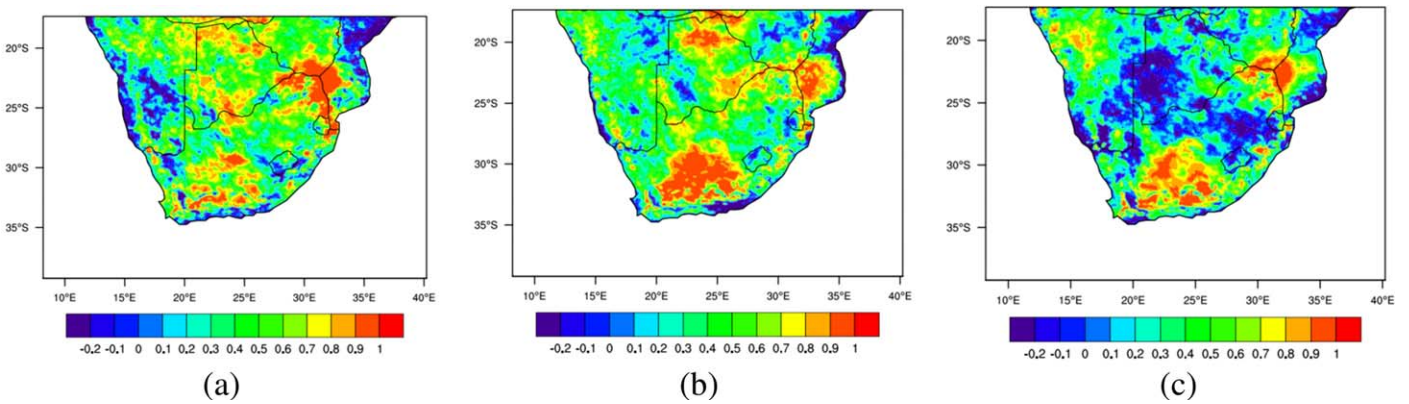

Figure 13. Observational Range Adjusted (ORA) temporal correlation of annual precipitation (mm) for (a) WRF_ERA-Iraw, (b) WRF_ERA-IcorrM, and (c) WRF_ERA-IcorrMSD.

the region using RegCM4 [*Li et al*., 2015; *Diallo et al*., 2014]. The largest wet biases over the Drakensburg and Lesotho were also revealed through the same study by *Moalafhi et al*. [2016b] where WRF was found to be sensitive to orographic forcing, as also revealed through other RCM studies over similar domains [*Kalognomu et al*., 2013; *Ratnam et al*., 2011]. Past studies over similar domain also revealed dry bias over Mozambique which was attributed to models overestimation of precipitation over Madagascar, to the east of the domain over the Indian ocean, and thus denying Mozambique the moisture column for precipitation. *Moalafhi et al*. [2016b] also showed that warm air masses frequently pass over Madagascar before reaching Mozambique.

5. Conclusions

Influence of bias correction of ERA-I reanalysis LBCs fields of atmospheric temperature and relative humidity using AIRS satellite data prior to downscaling has been investigated over a domain centered over southern Africa between the years 2003 and 2012. Two WRF downscaling experiments were undertaken; one using only mean-corrected and the other one using both mean and standard deviation corrected atmospheric temperature and relative humidity in the LBCs. To account for observational uncertainty, the simulations were evaluated against a collection of global gridded observational data sets. Mean bias, RMSE, and temporal correlation were derived seasonally and annually on simulated near-surface temperature and precipitation. These were compared with the raw ERA-I reanalysis (i.e., ERA-I reanalysis without any bias correction in the LBCs fields) driven WRF simulations to investigate the impact of the bias corrections on the model forced simulations over the domain.

Although bias correction of temperature and relative humidity LBC fields is impactful prior to downscaling, the resultant simulated climate does not show clear improvement. The bias correction produces mostly cooler and drier boundary conditions on average, but the resultant simulations show a generally warmer and wetter climate over the region. These imply that the more complex alternative bias correction procedures like the one suggested by *Mehrotra and Sharma* [2015] that maintains intervariable relationships and implemented recursively at different time scales should maybe be considered for future work. The current WRF model configuration might also need to be altered to make it more amenable to the influence of the lateral and lower boundary conditions. Since not all LBC variables (temperature, moisture, and winds) were corrected in this study, future work should consider inclusion of wind fields for improved simulations. All these might have implications not only for this particular domain and region of southern Africa. These challenges need to be addressed in future work to ensure that the best downscaled reanalysis data set is developed for use in hydrological impact studies over the region.

Similar to the WRF model's challenges in simulating temperature over the Namibian coastal plain and precipitation especially over complex topography [*Moalafhi et al*., 2016], the simulated climate with prior bias correction of the LBC variables also shows some anomalous warm temperature over the Namibian coastal plain and considerable wet bias over high-altitude areas. These appear to be a common challenge to RCMs over the region as revealed also in other previous studies.

Acknowledgments
We acknowledge funding support from the University of Botswana and the Australian Research Council (FT110100576 and FT100100197) that helped carry out this research. National Aeronautics and Space Administration (NASA) and National Oceanic and Atmospheric Administration (NOAA) provided AIRS satellite data and gridded observational data sets, respectively. ERA-I reanalysis was available from European Center for Medium range Weather Forecasting (ECMWF). This research was undertaken with the assistance of resources from the National Computational Infrastructure (NCI), which is supported by the Australian Government. All the model simulations and observational data sets they were evaluated against are available at https://unibots-my.sharepoint.com/personal/moalafhid_ub_ac_bw/_layouts/15/guestaccess.aspx?folderid=1b6de0338485f47d8b63ecb8054623474&authkey=AR2_rtJZod5QfkRolHGZrBA.

References

Adler, R. F., et al. (2003), The Version 2 Global Precipitation Climatology Project (GPCP) monthly precipitation analysis (1979-present), *J. Hydrometeorol.*, *4*, 1147–1167.

Aumann, H. H., et al. (2003), AIRS/AMSU/HSB on the Aqua Mission: Design, science objectives, data products and processing systems, *IEEE Trans. Geosci. Remote Sens.*, *41*, 253–264.

Bastola, S., and V. Misra (2014), Evaluation of dynamically downscaled reanalysis precipitation data for hydrological application, *Hydrol. Processes*, *28*(4), 1989–2002, doi:10.1002/hyp.9734.

Bates, B. C., Z. W. Kundzewicz, S. Wu, and J. P. Palutokof (Eds.) (2008), Climate change and water, in *Technical Paper of the Intergovernmental Panel on Climate Change*, 210 pp., IPCC Secretariat, Geneva.

Boulard, D., B. Pohl, J. Crétat, N. Vigaud, and T. Pham-Xuan (2012), Downscaling large-scale climate variability using a regional climate model: The case of ENSO over Southern Africa, *Clim. Dyn.*, *40*(5–6), 1141–1168, doi:10.1007/s00382-012-1400-6.

Colette, A., R. Vautard, and M. Vrac (2012), Regional climate downscaling with prior statistical correction of the global climate forcing, *Geophys. Res. Lett.*, *39*, L13707, doi:10.1029/2012GL052258.

Crétat, J., B. Pohl, Y. Richard, and P. Drobinski (2011a), Quantifying internal variability in a regional climate model: A case study of Southern Africa, *Clim. Dyn.*, *37*, 1335–1356, doi:10.1007/s00382-011-1021-5.

Crétat, J., B. Pohl, Y. Richard, and P. Drobinski (2011b), Uncertainties in simulating regional climate of Southern Africa: Sensitivity to physical parameterizations using WRF, *Clim. Dyn.*, *38*(3–4), 613–634, doi:10.1007/s00382-011-1055-8.

Diallo, I., F. Giorgi, S. Sukumaran, F. Stordal, and G. Giuliani (2014), Evaluation of RegCM4 driven by CAM4 over Southern Africa: Mean climatology, interannual variability and daily extremes of wet season temperature and precipitation, *Theor. Appl. Climatol.*, *121*, 749–766, doi:10.1007/s00704-014-1260-6.

Divakarla, M. G., C. D. Barnet, M. D. Goldberg, L. M. McMillin, E. Maddy, W. Wolf, L. Zhou, and X. Liu (2006), Validation of atmospheric infrared sounder temperature and water vapor retrievals with matched radiosonde measurements and forecasts, *J. Geophys. Res.*, *111*, D09S15, doi:10.1029/2005JD006116.

Druyan, L. M., and M. Fulakeza (2013), Downscaling reanalysis over continental Africa with a regional model: NCEP versus ERA Interim forcing, *Clim. Res.*, *56*(3), 181–196, doi:10.3354/cr01152.

Evans, J. P., and M. F. McCabe (2010), Regional climate simulation over Australia's Murray-Darling basin: A multitemporal assessment, *J. Geophys. Res.*, *115*, D14114, doi:10.1029/2010JD013816.

Evans, J. P., K. Bormann, J. Katzfey, S. Dean, and R. Arritt (2015), Regional climate model projections of the South Pacific Convergence Zone, *Clim. Dyn.*, *47*, 817–829.

Fan, Y., and H. van den Dool (2008), A global monthly land surface air temperature analysis for 1948–present, *J. Geophys. Res.*, *113*, D01103, doi:10.1029/2007JD008470.

Fetzer, E. J. (2006), Preface to special section: Validation of atmospheric infrared sounder observations, *J. Geophys. Res.*, *111*, D09S01, doi:10.1029/2005JD007020.

Fotso-Nguemo, T. C., et al. (2017), On the added value of the regional climate model REMO in the assessment of climate change signal over Central Africa, *Clim. Dyn.*, 1–26, doi:10.1007/s00382-017-3547-7.

Frei, C., J. H. Christensen, M. Déqué, D. Jacob, R. G. Jones, and P. L. Vidale (2003), Daily precipitation statistics in regional climate models: Evaluation and intercomparison for the European Alps, *J. Geophys. Res.*, *108*(D3), 4124, doi:10.1029/2002JD002287.

Hagemann, S., B. Machenhauer, R. Jones, O. B. Christensen, M. Déqué, D. Jacob, and P. L. Vidale (2004), Evaluation of water and energy budgets in regional climate models applied over Europe, *Clim. Dyn.*, *23*, 547–567.

Hao, Z., A. AghaKouchak, and T. J. Phillips (2013), Changes in concurrent monthly precipitation and temperature extremes, *Environ. Res. Lett.*, *8*(3), 034014, doi:10.1088/1748-9326/8/3/034014.

Kanamisu, M., and H. Kanamaru (2007), Scale-selective bias correction in a downscaling of global analysis using a regional model, *Mon. Weather Rev.*, *135*, 334–350.

Laprise, R., L. Hernández-Díaz, K. Tete, L. Sushama, L. Šeparović, A. Martynov, K. Winger, and M. Valin (2013), Climate projections over CORDEX Africa domain using the fifth-generation Canadian Regional Climate Model (CRCM5), *Clim. Dyn.*, *41*(11–12), 3219–3246, doi:10.1007/s00382-012-1651-2.

Legates, D., and C. Willmott (1990a), Mean seasonal and spatial variability in gauge-corrected, global precipitation, *Int. J. Climatol.*, *10*, 111–127.

Legates, D., and C. Willmott (1990b), Mean seasonal and spatial variability in global surface air temperature, *Theor. Appl. Climatol.*, *41*, 11–21.

Lélé, M. I., M. L. Lance, and P. J. Lamb (2015), Analysis of low-level atmospheric moisture transport associated with the West African Monsoon, *J. Clim.*, *28*(11), 4414–4430, doi:10.1175/jcli-d-14-00746.1.

Li, L., I. Diallo, C. Xu, and F. Stordal (2015), Hydrological projections under climate change in the near future by RegCM4 in Southern Africa using a large-scale hydrological model, *J. Hydrol.*, *528*, 1–16, doi:10.1016/j.jhydrol.2015.05.028.

Liang, X. Z., K. E. Kunkel, G. A. Meehl, R. G. Jones, and J. X. L. Wang (2008), Regional climate models downscaling analysis of general circulation models present climate biases propagation into future change projections, *Geophys. Res. Lett.*, *35*, L08709, doi:10.1029/2007GL032849.

Lin, J. L. (2007), Interdecadal variability of ENSO in 21 IPCC AR4 coupled GCMs, *Geophys. Res. Lett.*, *34*, L12702, doi:10.1029/2006GL028937.

Mehrotra, R., and A. Sharma (2012), An improved standardization procedure to remove systematic low frequency variability biases in GCM simulations, *Water Resour. Res.*, *48*, W12601, doi:10.1029/2012WR012446.

Mehrotra, R., and A. Sharma (2015), Correcting for systematic biases in multiple raw GCM variables across a range of timescales, *J. Hydrol.*, *520*, 214–225, doi:10.1016/j.jhydrol.2014.11.037.

Mehrotra, R., and A. Sharma (2016), A multivariate quantile-matching bias correction approach with auto- and cross-dependence across multiple time scales: Implications for downscaling, *J. Clim.*, *29*(10), 3519–3539.

Moalafhi, D. B., J. P. Evans, and A. Sharma (2016a), Evaluating global reanalysis datasets for provision of boundary conditions in regional climate modelling, *Clim. Dyn.*, *47* (9–10), 2727–2745, doi:10.1007/s00382-016-2994-x.

Moalafhi, D. B., J. P. Evans, and A. Sharma (2016b), Influence of reanalysis datasets on dynamically downscaling the recent past, *Clim. Dyn.*, 1–17, doi:10.1007/s00382-016-3378-y.

Mooney, P. A., R. Fealy, and F. J. Mulligan (2011), Comparison of ERA-Interim, ERA-40 and NCEP/NCAR reanalysis data with observed surface air temperatures over Ireland, *Int. J. Climatol.*, *31*, 545–557, doi:10.1002/joc.2008.

Pohl, B., M. Rouault, and S. R. Shouraseni (2014), Simulation of the annual and diurnal cycles of rainfall over South Africa by a regional climate model, *Clim. Dyn.*, *43*, 2207–2226, doi:10.1007/s00382-013-2046-8.

Ratna, S. B., J. V. Ratnam, S. K. Behera, C. J. de W. Rautenbach, T. Ndarana, K. Takahashi, and T. Yamagata (2013), Performance assessment of three convective parameterization schemes in WRF for downscaling summer rainfall over South Africa, *Clim. Dyn.*, *42*(11–12), 2931–2953, doi:10.1007/s00382-013-1918-2.

Ratnam, J. V., S. K. Behera, Y. Masumoto, K. Takahashi, and T. Yamagata (2011), A simple regional coupled model experiment for summer-time climate simulation over southern Africa, *Clim. Dyn.*, *39*(9–10), 2207–2217, doi:10.1007/s00382-011-1190-2.

Rawlins, M., R. Bradley, and H. Diaz (2012), Assessment of regional climate model simulation estimates over the northeast United States, *J. Geophys. Res.*, *117*, D23112, doi:10.1029/2012JD018137.

Sheffield, J., E. Wood, and M. Roderick (2012), Little change in global drought over the past 60 years, *Nature*, *491*, 435–438.

Skamarock, W. C., J. B. Klemp, J. Dudhia, D. O. Gill, D. M. Barker, M. G. Duda, X.-Y. Huang, W. Wang, and J. G. Powers (2008), A description of the advanced research WRF version 3, *NCAR Tech. Note NCAR/TN–475+STR*, Natl. Cent. for Atmos. Res., Boulder, Colo.

Susskind, J., C. Barnet, J. Blaisdell, L. Iredell, F. Keita, L. Kouvaris, G. Molnar, and C. Moustafa (2006), Accuracy of geophysical parameters derived from Atmospheric Infrared Sounder/Advanced Microwave Sounding Unit as a function of fractional cloud cover, *J. Geophys. Res.*, *111*, D09S17, doi:10.1029/2005JD006272.

Susskind, J., J. M. Blaisdell, and L. Iredell (2014), Improved methodology for surface and atmospheric soundings, error estimates, and quality control procedures: The atmospheric infrared sounder science team version-6 retrieval algorithm, *J. Appl. Remote Sens.*, *8*(1), 084994, doi:10.1117/1.jrs.8.084994.

Teutschbein, C., and J. Seibert (2012), Bias correction of regional climate model simulations for hydrological climate-change impact studies: Review and evaluation of different methods, *J. Hydrol.*, *456–457*, 12–29, doi:10.1016/j.jhydrol.2012.05.052.

Tobin, D. C., H. E. Revercomb, R. O. Knuteson, B. M. Lesht, L. L. Strow, S. E. Hannon, W. F. Feltz, L. A. Moy, E. J. Fetzer, and T. S. Cress (2006), Atmospheric radiation measurement site atmospheric state best estimates for Atmospheric Infrared Sounder temperature and water vapor retrieval validation, *J. Geophys. Res.*, *111*, D09S14, doi:10.1029/2005JD006103.

Vigaud, N., B. Pohl, and J. Crétat (2012), Tropical-temperate interactions over southern Africa simulated by a regional climate model, *Clim. Dyn.*, *39*(12), 2895–2916, doi:10.1007/s00382-012-1314-3.

Wood, A. W., L. R. Leung, V. Sridhar, and D. P. Lettenmaier (2004), Hydrologic implications of dynamical and statistical approaches to downscaling climate model outputs, *Clim. Change*, *62*(1–3), 189–216.

Xie, P., and P. A. Arkin (1997), Global precipitation: A 17-year monthly analysis based on gauge observations, satellite estimates, and numerical model outputs, *Bull. Am. Meteorol. Soc.*, *78*(11), 2539–2558.